Applied Catalysis B: Environmental 163 (2015) 9–15

Contents lists available at ScienceDirect

Applied Catalysis B: Environmental

journal homepage: www.elsevier.com/locate/apcatb

Synthesis of visible-light driven Cr_xO_y–TiO_2 binary photocatalyst based on hierarchical macro–mesoporous silica

Liujia Lu [a], Fei Teng [b], SenTapas [c], Dianyu Qi [a], Lingzhi Wang [a,*], Jinlong Zhang [a,*]

[a] Key Laboratory for Advanced Materials and Institute of Fine Chemicals, East China University of Science and Technology, 130 Meilong Road, Shanghai 200237, PR China

[b] Innovative Research Laboratory of Environment & Energy, Jiangsu Key Laboratory of Atmospheric Environment Monitoring & Pollution Control, School of Environmental Science and Engineering, Nanjing University of Information Science & Technology, Nanjing, PR China

[c] Centre for Materials Science, Institute of Nanotechnology and Bioengineering, School of Forensic and Investigative Sciences, University of Central Lancashire, Preston, UK

ARTICLE INFO

Article history:
Received 20 April 2014
Received in revised form 13 June 2014
Accepted 16 June 2014
Available online 21 June 2014

Keywords:
Hierarchical macro–mesoporous silica
Si–Cr–Ti
Visible-light driven photocatalysis

ABSTRACT

Hierarchical macro–mesoporous silica materials co-incorporated with Cr and Ti were directly synthesized by adopting close-packed array of polystyrene microsphere as hard template for macropore through a simple soaking-calcination way, where Si/Ti ratio was fixed at 200 and Si/Cr ratio was set between 200 and 10. Ti specie is highly dispersed in porous matrix and Cr specie mainly exists as tetra-coordinated CrO_3 at higher Si/Cr ratio (Si/Cr ≥ 50), which transforms to a mixture of CrO_3 and crystallized hexa-coordinated Cr_2O_3 when Si/Cr ratio is below 50. This highly interconnected porous material co-incorporated with Cr and Ti presents highest visible-light driven photocatalytic activity at Si/Cr = 20 toward degradation of AO7. Moreover, macro–mesoporous photocatalyst presents higher activity than those of macroporous and mesoporous ones at the same Si/Cr ratio. The improved visible light driven catalytic activity is mainly attributed to effective metal to metal charge transfer from Cr(VI) to Ti(IV) benefitted from the uniform dispersion of these two species in hierarchical porous silica matrix.

1. Introduction

Recently, hierarchically porous materials with interconnected binary pore system and highly tunable pore size over different length scales [1–6] have been widely used for energy conversion [7], sensor devices [8,9], separation [10] and catalysis [11]. Among them, inverse opal macroporous–mesoporous structures with macroporous window and mesoporous skeleton have attracted more attention due to their uniformly arranged macroporous voids, which often leads to unique performance on photonic modulation and mass transfer [11,12]. Generally, hierarchically porous materials composed of macroporous and mesoporous systems are synthesized through a dual-template system using colloidal particle with uniform size as hard template for macropore and long-chain surfactant as soft template for mesopore [13–15]. Silica or polymer microspheres including polystyrene (PS) and poly(methyl methacrylate) (PMMA)are often adopted as hard templates [16–20], which generally assemble into a uniform and close-packed array before casting of mesoporous precursor through a dip-coating or spin-coating method. A macroporous–mesoporous inverse opal can be obtained after the removal of hard template through a dissolution or calcination way. The macropore and mesopore sizes can be, respectively, tuned by adopting appropriate hard and soft templates [21,22].

Recently, hierarchically porous material has attracted considerable attention from the field of photocatalysis owing to its highly interconnected and accessible pore structure [23–25]. Hierarchical photocatalysts with different components such as TiO_2, WO_3 and Bi_2WO_6 have been reported [26–28]. Among them, silica based hierarchical photocatalyst loaded with highly dispersed semiconductor nanoparticle or nanocluster have drawn increasingly attention due to its more ordered pore structure and larger specific surface area than its metal oxide counterparts [29]. When loaded on matrix with large specific surface area, the agglomeration of nano-photocatalyst can be effectively inhibited, which is beneficial to the improvement of photocatalytic activity due to the

* Corresponding authors at: East China University of Science and Technology, Key Laboratory for Advanced Materials and Institute of Fine Chemicals, 130, Meilong Road, Shanghai 200237, PR China. Tel.: +086 021 64252062.
E-mail addresses: wlz@ecust.edu.cn (L. Wang), jlzhang@ecust.edu.cn (J. Zhang).

http://dx.doi.org/10.1016/j.apcatb.2014.06.024
0926-3373/

more easily separable photo-generated electron–hole pair [30,31]. However, this advantage is actually achieved at the expense of light-absorption range of photocatalyst. For example, the high dispersion of Ti species in silica framework increases splitting degree of energy lever, leading to the widening of forbidden band and the blue-shift of absorption spectrum [32]. In order to enhance visible light absorption ability, transition metal (V, Mo, Cr etc) was incorporated into framework of mesoporous silica besides Ti [33,34]. For examples, Guo [35] and Shiraishi et al. [36] co-introduced Cr and Ti species into silica and achieved visible light driven photocatalytic activity from metal-to-metal charge-transfer (MMCT) excitation of oxo-bridged bimetallic units (Cr–O–Ti). Hashimoto [37] introduced hetero-bimetallic Ti(IV)–O–Ce(III) assemblies into pore channel of mesoporous silica, leading to the formation of visible light active photocatalyst. However, up to now, there are still fewer reports about the fabrication of bimetallic assembly based on hierarchical porous system.

Herein, we reported the fabrication visible-light responsive photocatalyst based on inverse opal mesoporous silica co-incorporated with Ti and Cr through a simple soaking-calcination way. Inverse opal mesoporous silica is chosen in consideration of its highly interconnected hierarchical pore structure as mentioned above. The influences of macroporous structure and the existing form of Cr species to the photocatalytic activity were specifically studied. The mechanism for the improved photocatalytic activity was finally proposed based on a systematically comparative study about the effect of different porous structures and Si/Cr ratios.

2. Experimental

2.1. Fabrication of different Si–Cr–Ti photocatalysts

Monodisperse PS spheres and the PS photonic crystals were synthesized as described previously [38]. For the preparation of MM–Si–Cr–Ti, 2.2 mL tetraethylorthosilicate (TEOS), 17 mg tetrabutyltitanate (TBOT) and 2.5 mg acetylacetone (AcAc) were mixed together for 30 min (the molar ratios of TBOT/AcAc = 2/1). At the same time, 1.0 g F127, 0.1 mL HCl (2 M/L) and 0.8 mL deionized water were dissolved in 16 mL ethanol at 40 °C. After stirring at 25 °C for 1 h, 0.04 g (0.08 g, 0.2 g and 0.4 g) $Cr(NO_3)_3{\cdot}9H_2O$ was added and then the mixture was continuously stirred until the solution was clear. To it, the mixtures of TEOS, TBOT and AcAc were added and then the mixture was continuously stirred at 60 °C for 1 h. The molar ratios of Si/Cr/Ti are 200/(2, 4, 10 and 20)/1. Afterward, the PS photonic crystals were immersed into the mesoporous precursor solution. The samples were left to air dry overnight at 25 °C, and were then calcined under air flow to remove the templates, leading to the formation of MM–Si–Cr–Ti. The calcination temperature was increased from 25 °C to 500 °C with a ramp of 2 °C/min and maintained at 500 °C for 4 h. For comparison, Me–Si–Cr–Ti and Ma–Si–Cr–Ti samples were synthesized according to the above procedure without PS photonic crystals or F127 templates.

On the other hand, TiO_2/MM–Si–Cr was prepared by introducing Ti species into MM–Si–Cr with a post treatment method. Specifically, MM–Si–Cr was first fabricated using the procedure for MM–Si–Cr–Ti except the absence of TBOT and AcAc in the precursor solution. Subsequently, TBOT and AcAc were dissolved in 10 mL ethanol at 25 °C for 15 min. MM–Si–Cr powders was dispersed in the solution and continuously stirred at 25 °C for 2 h. After the evaporation of ethanol, the samples were then heated at a speed of 2 °C/min to 500 °C and held at this temperature for 4 h. The molar ratio of Ti/Si in the precursor solution for the preparation of TiO_2/MM–Si–Cr was equal to that of MM–Si–Cr–Ti.

Table 1
Element weight percentage of MM–Si–Cr–Ti materials.

element	O	Si	Cr	Ti	Total
Si/Cr = 10	45.31	43.70	10.55	0.44	100
Si/Cr = 20	44.91	49.92	4.71	0.46	100
Si/Cr = 50	44.65	52.73	2.15	0.47	100
Si/Cr = 100	44.98	53.43	1.12	0.47	100

2.2. Characterization

X-ray diffraction (XRD) patterns of the samples were recorded on a Rigaku D/MAX-2550 diffractometer using Cu $K\alpha$ radiation of wavelength 1.5406 Å, typically running at a voltage of 40 kV and current of 100 mA. UV–vis absorbance spectra were achieved for the dry-pressed disk samples using a Scan UV–vis spectrophotometer (Varian, Cary 500) equipped with an integrating sphere assembly, using $BaSO_4$ as a reflectance sample. Scanning electron microscopy (SEM) images were obtained with a JEOL JSM-6360LV microscope at an accelerating voltage of 15 kV. Transmission electron microscopy (TEM) images were collected on a JEOL JEM 2010F, electron microscope operated at an acceleration voltage of 200 kV. By utilizing the Barrett–Joyner–Halenda (BJH) model, the pore volumes and pore size distributions were got from the adsorption branches of isotherms. Electron paramagnanetic resonance (EPR) spectra were recorded on Varian E-112 at 77 K. Catalyst (50 mg) was placed in a quartz EPR tube and placed on the EPR sample cavity after photoirradiated20 min using 300 W xenon lamp at $\lambda > 400$ nm (with filter).

2.3. Photocatalytic testing

Typically, 40 mg catalyst was added to an aqueous suspension of AO7 (40 mL, 10 mg/L) in a glass tube with vigorously magnetic stirring. The illuminated light source comes from a 300 W xenon lamp equipped with a cut-off filter to ensure the wavelengths more than 420 nm. Every hour the above suspension (about 5 mL) was extracted from the mixture solution during visible-light irradiation. The change of concentration of AO7 was tested by the Cary 100 UV–vis spectrometer.

3. Results and discussion

The hierarchical porous silica co-incorporated with Cr and Ti was obtained by a method simply combing soaking and calcination treatments, where the washing and centrifugation procedures were avoided. Such a synthesis system is advantageous to the minimization of material loss generally found in other synthesis system. The compositions of different MM–Si–Cr–Ti samples analyzed by ICP-AES indicate the actual contents of Cr and Ti species are accordant with their initial concentrations in precursor solutions (Table 1), which well illustrates that the preparation method presented here is effective to avoid material loss.

Scan electron microscopy (SEM) shows PS fabricated through a vertical deposition method adopts highly ordered close-packed arrangement (Fig. 1a). An interconnected macroporous network is formed through a soaking-calcination process (Fig. 1b), where the size of the macropore is well accordant with that of PS. This result indicates that the diameter of the macropores can be well duplicated from PS particle. Transmission electron microscopy (TEM) images (Fig. 1c and d) indicate the wall of the macropore system is composed of interconnected mesopores. Such a highly interconnected and open hierarchical porous system makes MM–Si–Cr–Ti excellent carrier for the dispersion of guest molecules.

The formation of mesoporous structure is further confirmed by low-angle X-ray diffraction (XRD) patterns and N_2

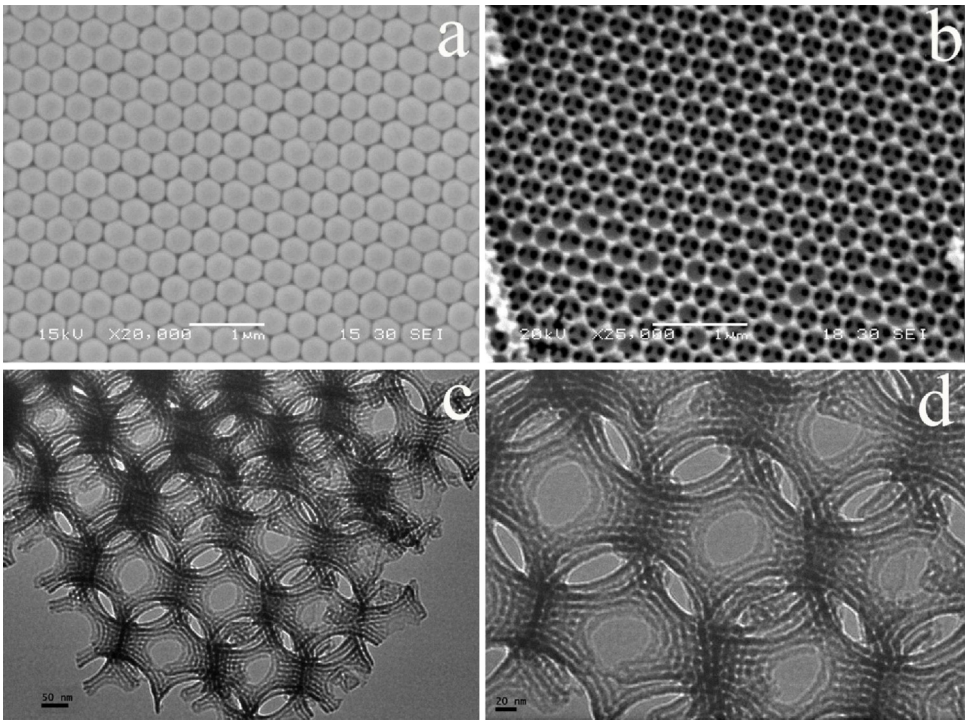

Fig. 1. SEM (a and b) and TEM (c and d) images of MM–Si–Cr–Ti prepared at molar ratio of Si/Cr/Ti = 200/10/1.

adsorption-desorption isotherms (Fig. 2a and b). All of samples show a broad diffraction peak attributed to mesoporous characteristics except for the sample prepared at Si/Cr = 10 (Fig. 2a), which indicates a high concentration of Cr in the synthesis system may severely interrupt the formation of mesoporous structure [39,40]. N_2 sorption isotherms show typical type IV isotherm with pronounced H_2 hysteresis loops and distinct jump at a higher relative pressure above 0.8, verifying the co-existence of macropore and mesopore (Fig. 2b).

The diffuse reflectance UV-vis spectra of MM–Si–Cr samples (Fig. 3a) and MM–Si–Cr–Ti samples (Fig. 3b) indicate no obvious absorption is observed from pure siliceous sample, while UV bands at 280 nm and 370 nm are found in Cr-incorporated samples, which are usually assigned to O → Cr(VI) charge transfer of chromate species in tetrahedral coordination [41]. A weak shoulder peak around 440 nm can be assigned to Cr(VI) polychromate [42]. Moreover, a peak between 600 and 700 nm attributed to d–d transition of octahedral Cr(III) gradually increases with the decreasing Si/Cr ratio, indicating the formation of Cr_2O_3 nanocluster in the pore channel at lower Si/Cr ratio [6,41,43]. A comparison between MM–Si–Cr–Ti and MM–Si–Cr samples indicates a new peak appears at about 250 nm, which is obviously much shorter than the maximum absorption wavelength of TiO_2 nanocrystallite and can be assigned to the ligand-to-metal charge transfer (LMCT) absorption of highly dispersed Ti species [44,45]. No peak attributed to TiO_2 crystallite is found from the wide-angle XRD patterns of MM–Si–Cr–Ti samples (Fig. 3d) prepared with different Si/Cr ratios, which only show increased peak intensity of Cr_2O_3 nanocrystal with decreasing Si/Cr ratio. Raman spectrum of dehydrated MM–Si–Cr–Ti and MM–Si–Cr are further used to detect the actual state of Ti species (Fig. 3c). The broad Raman band at 1080 cm^{-1} of sample MM–Si–Cr–Ti can be assigned to silica vibrations perturbed by the presence of Ti, which indicates the existence of Si–O–Ti bonds [46]. Moreover, there is no band ascribed to rutile or anatase phase, which further excludes the presence of TiO_2 clusters. These results indicate that MM–Si–Cr–Ti samples prepared through a soaking-calcination way can actually form highly dispersed Cr(VI) and Ti(IV) oxide species by choosing appropriate Si/Cr ratio.

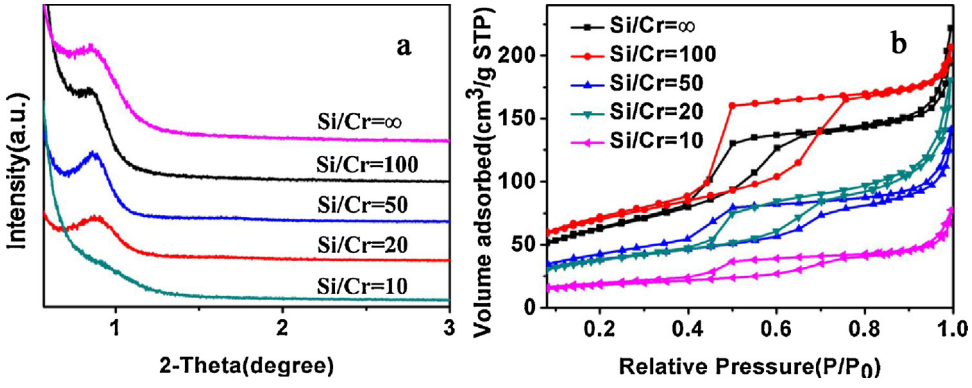

Fig. 2. (a) Low-angle XRD patterns and (b) N_2 adsorption/desorption isotherms of MM–Si–Cr–Ti samples with different Si/Cr molar ratios.

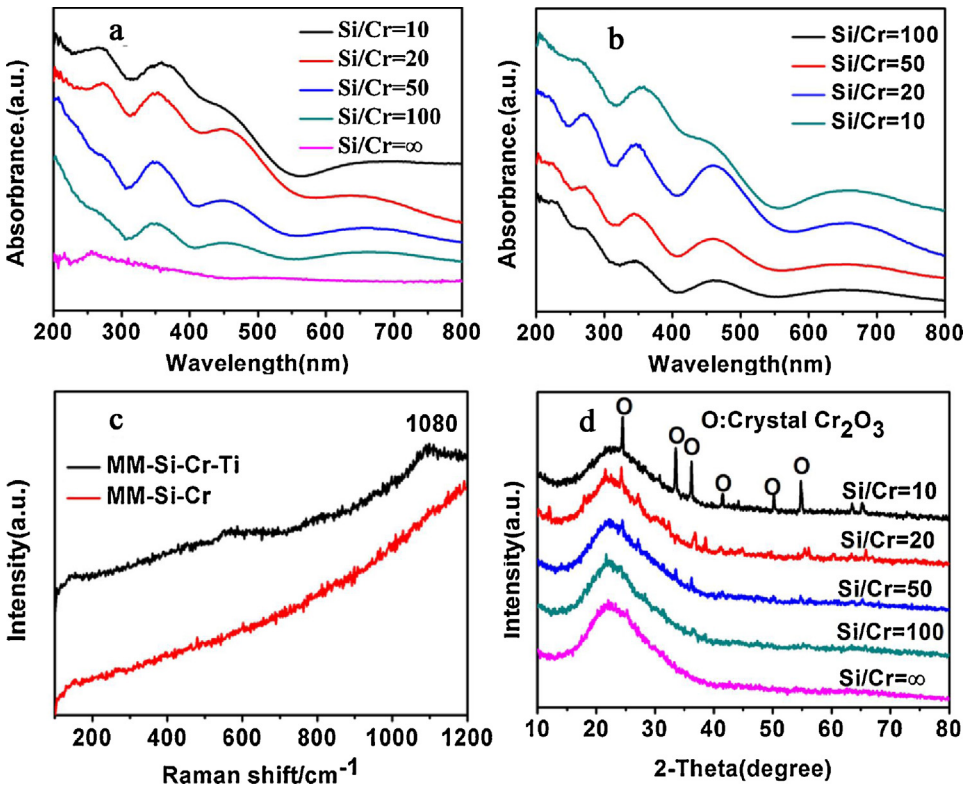

Fig. 3. (a) UV–vis diffuse reflectance spectra of MM–Si–Cr samples; (b) UV–vis diffuse reflectance spectra of MM–Si–Cr–Ti samples; (c) Raman spectra of MM–Si–Cr–Ti and MM–Si–Cr samples; (d) Wide-angle XRD patterns MM–Si–Cr–Ti samples prepared at different Si/Cr molar ratios.

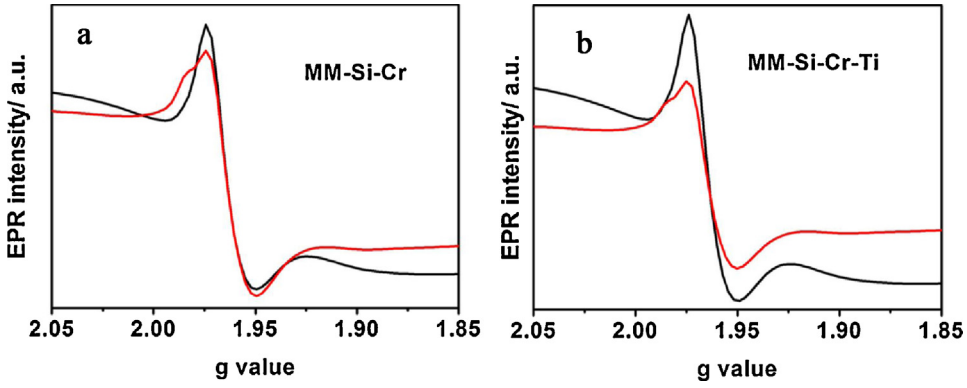

Fig. 4. EPR spectra (77 K) of (a) MM–Si–Cr and (b) MM–Si–Cr–Ti samples measured before photoirradiation (black) and after photoirradiation (red). The Si/Cr ratio is 100. (For interpretation of the references to color in this figure legend, the reader is referred to the web version of this article.)

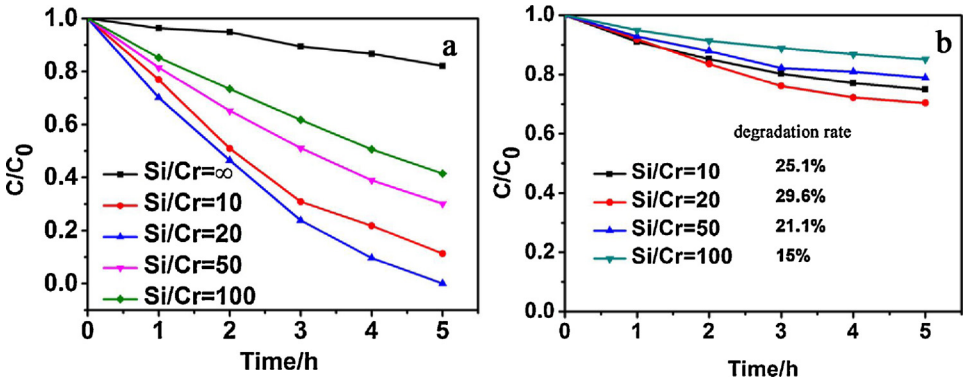

Fig. 5. Photocatalytic activity of (a) MM–Si–Cr–Ti samples and (b) MM–Si–Cr samples prepared at different Si/Cr molar ratios for the degradation of AO7 under visible light illumination.

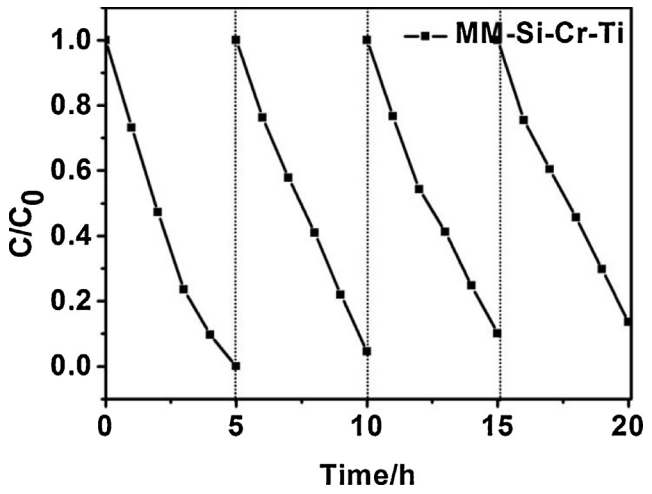

Fig. 6. Recycling photocatalytic degradation of AO7 under visible-light illumination with MM–Si–Cr–Ti (Si/Cr = 20).

To confirm the interaction between Cr and Ti species, electron paramagnetic resonance (EPR) was further used to study the signal of Cr species in MM–Si–Cr and MM–Si–Cr–Ti. The signals at $g_{\perp} = 1.975$ and $g_{||} = 1.952$ are assigned to Cr(V) reduced from Cr(VI) by vacuo treatment before EPR analysis (Fig. 4) [47]. After the photoirradiation, the transferring of photoinduced electron from oxygen atom to Cr(V) leads to the formation of excited Cr(IV), so the signal intensity of Cr(V)decreases. Compared with that of MM–Si–Cr (Fig. 4a), the intensity of Cr(V) in MM–Si–Cr–Ti (Fig. 4b) reduces more significantly, verifying the interaction between Cr and Ti. Similar findings have been reported from oxo-bridged Cr(V)–O–Ti(IV) species due to the charge transfer through bridging oxygen, leading to the formation of excited Cr(IV)–O–Ti(III) [36,48].

The photocatalytic activity of MM–Si–Cr–Ti samples for the degradation of AO7 was studied under visible-light irradiation. It is obvious that sample only doped with Ti specie shows negligible visible-light responsive activity due to the wide forbidden band of titanium oxide (Fig. 5a). However, the activity is significantly improved when only tiny amount of Cr species is introduced to sample prepared at a high Si/Cr ratio of 100. The photocatalytic activity increases with the decreasing Si/Cr ratio from 100 to 20. However, it cannot be further improved when Si/Cr ratio continuously decreases to 10. All of MM–Si–Cr samples only with Cr species show much lower visible-light driven photocatalytic activity than those of MM–Si–Cr–Ti (Fig. 5b). Moreover, recycling study on MM–Si–Cr–Ti prepared at Si/Cr ratio = 20 shows it can maintain initial photocatalytic activity after 4 cycles (Fig. 6), indicating the good stability of MM–Si–Cr–Ti photocatalyst.

Subsequently, the photocatalytic activity of Si–Cr–Ti samples with different porous system was compared to clarify the effect of pore structure. MM–Si–Cr–Ti materials obviously exhibit higher degradation percentage for AO7 than Ma–Si–Cr–Ti only with macroporous structure or Me–Si–Cr–Ti only with mesoporous structure (Fig. 7a). The photodegradation of AO7 follows first-order kinetics, where the rate constant on MM–Si–Cr–Ti is much higher than that on Me–Si–Cr–Ti and Ma–Si–Cr–Ti (Fig. 7b–d). Results from N_2 adsorption/desorption analysis indicate MM–Si–Cr–Ti shows higher specific surface area than that of Ma–Si–Cr–Ti only with macropore, and larger pore volume and size than MM–Si–Cr–Ti only with mesopore (Table 2). Therefore, the improved photocatalytic activity can be partly ascribed to more efficient diffusion of AO7 molecules in hierarchical porous system during photocatalytic process [14]. Besides, the ordered macroporous structure leads to more effective light absorption by multiple light scattering [49,50], which is advantageous to the improvement of light absorption efficiency.

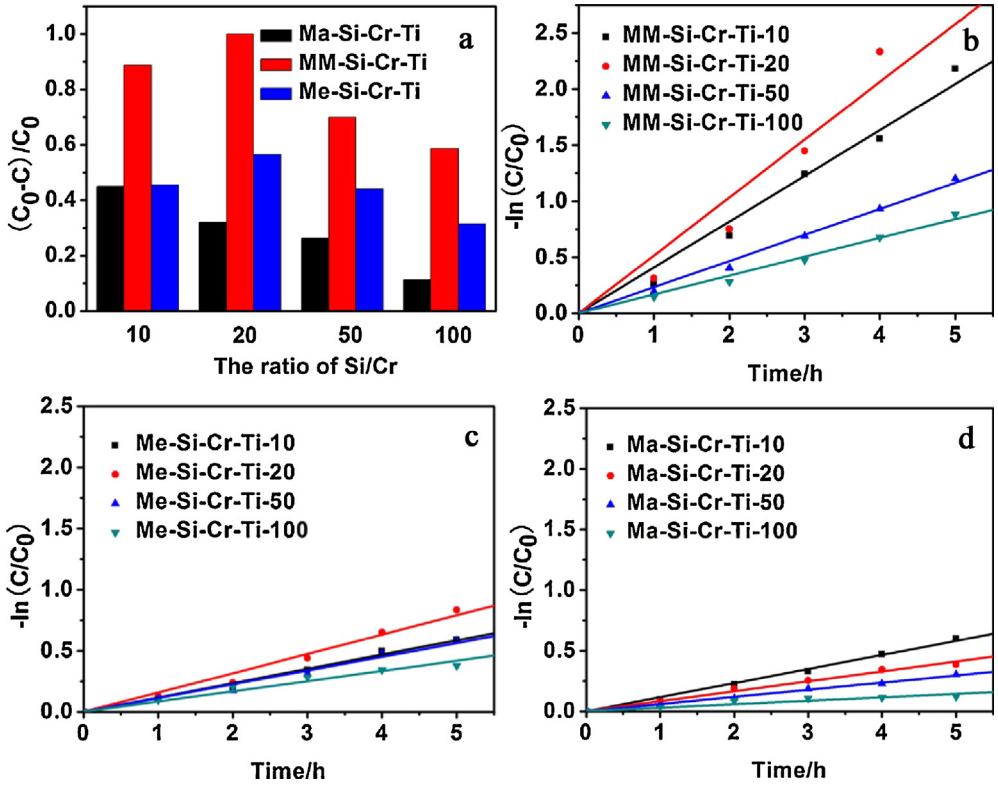

Fig. 7. (a) Photocatalytic degradation percentages of AO7 under visible light irradiation with Ma–Si–Cr–Ti, MM–Si–Cr–Ti and Me–Si–Cr–Ti; (b, c and d) Photocatalytic kinetic curves of AO7 under visible light irradiation with MM–Si–Cr–Ti–*X*, Me–Si–Cr–Ti–*X* and Ma–Si–Cr–Ti–*X*, respectively, where *X* represents the ratios of Si/Cr.

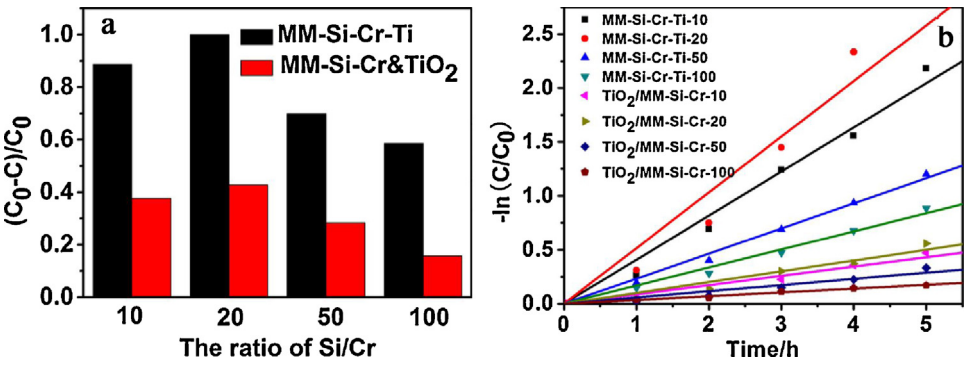

Fig. 8. (a) Photocatalytic degradation percentages and (b) kinetic curves of AO7 under visible light irradiation with MM–Si–Cr–Ti andTiO_2/MM–Si–Cr.

To better understand the effect of Ti–O–Cr, the visible-light driven photocatalytic activity (Fig. 8a) and the first-order kinetic curve (Fig. 8b) of MM–Si–Cr–Ti catalysts was further compared with TiO_2/MM–Si–Cr, where Ti species was introduced through a post treatment method [51]. It is obvious that MM–Si–Cr–Ti shows higher activity than TiO_2/MM–Si–Cr. It is possible that the loading of Ti species through a post treatment results in the formation of less dispersed Ti species, making its contact with Cr oxides less efficient and leading to the decrease of visible-light responsive activity.

Moreover, the photocatalytic activity of MM–Si–Cr–Ti samples for the degradation of AO7 under UV irradiation was also investigated (Fig. 9). Compared with the results from visible light irradiation, it is found that the catalysts show poorer UV-light driven activities, which seems not much influenced by the increasing content of Cr. The results well illustrate that Ti specie plays a dominant role in UV-light irradiated photocatalysis, while oxo-bridged Cr–O–Ti species is the key factors for visible-light irradiated one.

Based on the above results, we suggest the improved visible-light driven photocatalytic activity of MM–Si–Cr–Ti co-incorporated with Cr and Ti should be related to the visible light absorption ability of Cr species, good interaction between Cr and Ti and highly accessible pore system. However, the specific functions of Cr(VI) and Cr(III) seem still ambiguous. Cr species is highly dispersed in silica matrix as isolated Cr(VI) at a low Cr content (Si/Cr = 100), which means the visible-light driven activity of sample prepared at Si/Cr = 100 is initiated from MMCT from Cr(VI) to Ti(IV) [37]. The decreasing of Si/Cr ratio from 100 to 20 gradually leads to the increasing of Cr content mainly in the forms of oligomeric Cr(VI), resulting in further improved photocatalytic activity. The formation of Cr_2O_3 nanocluster can effectively extend the absorption range to 700 nm. It cannot be excluded that the excited Cr_2O_3 cluster may donate electron to neighboring TiO_2 according to their energy level of conduction band. However, the formation of Cr_2O_3 simultaneously leads to severe deterioration of pore structure as found from small-angle XRD pattern, which makes the effect of Cr_2O_3 on the photocatalytic efficiency ambiguous since the pore disordering caused by the formation of Cr_2O_3 cluster is definitely disadvantageous to the photocatalytic application. However, no matter whether the absorption of Cr_2O_3 is positive to the photocatalysis activity or not, the pore deterioration caused by the formation of Cr_2O_3 proves to have a dominant interruption effect on photocatalytic efficiency according to the decreased photocatalytic activity with the increasing amount of Cr_2O_3 cluster from Si/Cr = 20 to 10.

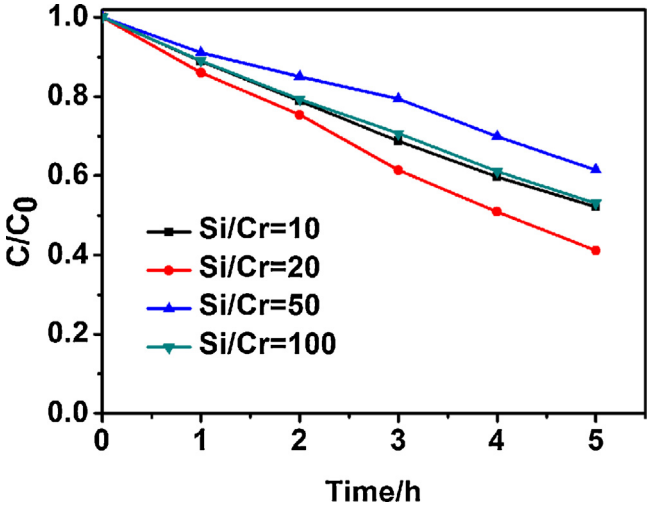

Fig. 9. Photocatalytic activity of MM–Si–Cr–Ti prepared with different Si/Cr molar ratios for the degradation of AO7 under UV irradiation.

Table 2
Structural and textural parameters of samples Ma–Si–Cr–Ti, MM–Si–Cr–Ti and Me–Si–Cr–Ti.

Sample[a]	S_{BET}[b]	V_t[c]	D_{pa}[d]	D_{pd}[e]
	(m^2/g)	(cm^3/g)	(nm)	(nm)
Ma–Si–Cr–Ti	74	0.091	–	–
MM–Si–Cr–Ti	255	0.31	5.1	4.6
Me–Si–Cr–Ti	280	0.26	4.5	3.7

[a] All of three porous samples are prepared at Si/Cr/Ti = 200/10/1.
[b] S_{BET} is the specific surface area measured from N_2 physisorption.
[c] V_t is the pore volume measured at $P/P_o = 0.99$.
[d] D_{pa} is the pore size calculated from N_2 sorption isotherm based on BJH model from adsorption branches.
[e] D_{pd} is the pore size calculated from N_2 sorption isotherm based on BJH model from desorption branches.

4. Conclusions

In summary, we demonstrate a simple soaking-calcination method to synthesize hierarchical macro–mesoporous silica based photocatalyst MM–Si–Cr–Ti. The highly interconnected and accessible porous structure and the effective interaction between uniformly dispersed Cr(VI) and Ti(IV) species make MM–Si–Cr–Ti more catalytically active under visible light irradiation than macroporous Ma–Si–Cr–Ti, mesoporous Me–Si–Cr–Ti and TiO_2/MM–Si–Cr. The good recyclability of MM–Si–Cr–Ti further proves the superiority of this hierarchical photocatalyst. We believe such a simple way for fabrication of visible-light responsive photocatalyst with hierarchical interconnected porous structure will find more applications in photocatalysis field.

Author information

The authors declare no competing financial interest.

Acknowledgments

This work has been supported by the National Natural Science Foundation of China (21173077, and 21237003); the National Basic Research Program of China (973 Program, 2013CB632403); the Project of International Cooperation of the Ministry of Science and Technology of China (No. 2011DFA50530); Science and Technology Commission of Shanghai Municipality (12230705000, 12XD1402200); the Research Fund for the Doctoral Program of Higher Education (20120074130001); Open Project from Jiangsu Key Laboratory of Atmospheric Environment Monitoring and Pollution Control of Nanjing University of Information Science and Technology (kHK1110), Jiangsu Province Innovation Platform for Superiority Subject of Environmental Science and Engineering.

References

[1] K. Kanamori, K. Nakanishi, Chem. Soc. Rev. 40 (2011) 754–770.
[2] Z. Sun, Y. Deng, J. Wei, D. Gu, B. Tu, D. Zhao, Chem. Mater. 23 (2011) 2176–2184.
[3] G.L. Drisko, M. Chee Kimling, N. Scales, A. Ide, E. Sizgek, R.A. Caruso, V. Luca, Langmuir 26 (2010) 17581–17588.
[4] A. Lemaire, B.-L. Su, Langmuir 26 (2010) 17603–17616.
[5] T.Y. Ma, Z.Y. Yuan, Eur. J. Inorg. Chem. 2010 (2010) 2941–2948.
[6] B.M. Weckhuysen, L.M. De Ridder, R.A. Schoonheydt, J. Phys. Chem. 97 (1993) 4756–4763.
[7] C.M. Doherty, R.A. Caruso, B.M. Smarsly, C.J. Drummond, Chem. Mater. 21 (2009) 2895–2903.
[8] Y.J. Lee, C.E. Heitzman, W.R. Frei, H.T. Johnson, P.V. Braun, J. Phys. Chem. B 110 (2006) 19300–19306.
[9] R.A. Barry, P. Wiltzius, Langmuir 22 (2005) 1369–1374.
[10] K. Nakanishi, N. Tanaka, Acc. Chem. Res. 40 (2007) 863–873.
[11] J. Zhao, F. Cheng, C. Yi, J. Liang, Z. Tao, J. Chen, J. Mater. Chem. 19 (2009) 4108–4116.
[12] J. Lei, L. Wang, J. Zhang, ACS Nano 5 (2011) 3447–3455.
[13] Y. Deng, C. Liu, T. Yu, F. Liu, F. Zhang, Y. Wan, L. Zhang, C. Wang, B. Tu, P.A. Webley, H. Wang, D. Zhao, Chem. Mater. 19 (2007) 3271–3277.
[14] M. Xu, D. Feng, R. Dai, H. Wu, D. Zhao, G. Zheng, Nanoscale 3 (2011) 3329–3333.
[15] L. Samiee, A. Beitollahi, Res. Chem. Intermed. (2013) 1–17.
[16] O.D. Velev, T.A. Jede, R.F. Lobo, A.M. Lenhoff, Nature 389 (1997) 447–448.
[17] A. van Blaaderen, Science 282 (1998) 887–888.
[18] J.E.G.J. Wijnhoven, S.J.M. Zevenhuizen, M.A. Hendriks, D. Vanmaekelbergh, J.J. Kelly, W.L. Vos, Adv. Mater. 12 (2000) 888–890.
[19] J.D. Joannopoulos, Nature 414 (2001) 257–258.
[20] T. Kamegawa, N. Suzuki, H. Yamashita, Chem. Lett. 38 (2009) 610–611.
[21] Y. Liu, L. Wang, J. Zhang, F. Chen, M. Anpo, Res. Chem. Intermed. 37 (2011) 949–959.
[22] Y. Wang, G. Chen, F. Zhang, L. Li, Res. Chem. Intermed. 40 (2014) 385–397.
[23] T. Yan, L. Li, G. Li, Res. Chem. Intermed. 37 (2011) 297–307.
[24] J.G. Yu, Y.R. Su, B. Cheng, Adv. Funct. Mater. 17 (2007) 1984–1990.
[25] F. Lu, W. Cai, Y. Zhang, Adv. Funct. Mater. 18 (2008) 1047–1056.
[26] T. Kamegawa, N. Suzuki, M. Che, H. Yamashita, Langmuir 27 (2011) 2873–2879.
[27] Z. Gu, T. Zhai, B. Gao, X. Sheng, Y. Wang, H. Fu, Y. Ma, J. Yao, J. Phys. Chem. B 110 (2006) 23829–23836.
[28] M. Shang, W. Wang, L. Zhang, S. Sun, L. Wang, L. Zhou, J. Phys. Chem. C 113 (2009) 14727–14731.
[29] E. Mehrasbi, Y. Sarrafi, A. Vahid, H. Alinezhad, Res. Chem. Intermed. (2014) 1–13, http://dx.doi.org/10.1007/s 11164-014-1578-9.
[30] B.I. Park, H. Jie, B.G. Song, K.M. Kang, J.K. Park, S.H. Cho, Res. Chem. Intermed. 40 (2014) 115–126.
[31] L. Jiang, L. Wang, J. Zhang, Chem. Commun. 46 (2010) 8067–8069.
[32] L. Samiee, A. Beitollahi, M. Bahmani, M.M. Akbarnejad, A. Vinu, Res. Chem. Intermed. 36 (2010) 897–923.
[33] Y. Shao, L. Wang, J. Zhang, M. Anpo, J. Phys. Chem. B 109 (2005) 20835–20841.
[34] H. Liu, Y. Wu, J. Zhang, ACS Appl. Mater. Interfaces 3 (2011) 1757–1764.
[35] S. Shen, L. Guo, Catal. Today 129 (2007) 414–420.
[36] D. Tsukamoto, A. Shiro, Y. Shiraishi, T. Hirai, J. Phys. Chem. C 115 (2011) 19782–19788.
[37] R. Nakamura, A. Okamoto, H. Osawa, H. Irie, K. Hashimoto, J. Am. Chem. Soc. 129 (2007) 9596–9597.
[38] S.E. Shim, Y.J. Cha, J.M. Byun, S. Choe, J. Appl. Polym. Sci. 71 (1999) 2259–2269.
[39] B. Sun, E.P. Reddy, P.G. Smirniotis, Appl. Catal., B: Environ. 57 (2005) 139–149.
[40] B. Sun, E.P. Reddy, P.G. Smirniotis, J. Catal. 237 (2006) 314–321.
[41] B.M. Weckhuysen, I.E. Wachs, R.A. Schoonheydt, Chem. Rev. 96 (1996) 3327–3350.
[42] K. Takehira, Y. Ohishi, T. Shishido, T. Kawabata, K. Takaki, Q. Zhang, Y. Wang, J. Catal. 224 (2004) 404–416.
[43] E. Groppo, C. Lamberti, S. Bordiga, G. Spoto, A. Zecchina, Chem. Rev. 105 (2005) 115–184.
[44] X. Gao, S.R. Bare, J.L.G. Fierro, M.A. Banares, I.E. Wachs, J. Phys. Chem. B 102 (1998) 5653–5666.
[45] S. Bordiga, S. Coluccia, C. Lamberti, L. Marchese, A. Zecchina, F. Boscherini, F. Buffa, F. Genoni, G. Leofanti, J. Phys. Chem. 98 (1994) 4125–4132.
[46] X. Gao, S.R. Bare, J. Fierro, M.A. Banares, I.E. Wachs, J. Phys. Chem. B 102 (1998) 5653–5666.
[47] B.M. Weckhuysen, R.A. Schoonheydt, F.E. Mabbs, D. Collison, J. Chem Soc, Faraday Trans. 92 (1996) 2431–2436.
[48] S. Rodrigues, K.T. Ranjit, S. Uma, I.N. Martyanov, K.J. Klabunde, Adv. Mater. 17 (2005) 2467–2471.
[49] K. Sakoda, Opt. Express 4 (1999) 167–176.
[50] A. Imhof, W.L. Vos, R. Sprik, A. Lagendijk, Phys. Rev. Lett. 83 (1999) 2942.
[51] L.Z. Wang, L. Jiang, C.C. Xu, J.L. Zhang, J. Phys. Chem. C 116 (2012) 16454–16460.